2

Chapter 2

Heat and Partial Slip Impact on Elastico-Viscous Fluid Flow Past a Flat Permeable Plate

2.1 Introduction

The elastico-viscous fluid has little temperature and salinity sensitivity, and is easily regulated by rheology. The elastico-viscous fluid technology generates highly efficient fractures with low damage to conductivity providing excellent control of fluid loss and high properties of proppant transport to generate geometry of design fractures. The rheology of elastico-viscous fluid are used to enhance biomodeling. Biofilms are also elastico-viscous materials that are capable of dissipating energy from external forces and overcoming external mechanical stresses.

The fluid motion of the elastico-viscous boundary layer through a permeable surface. surface along with heat transport in presence of partial slip has influenced researchers a lot these days. This flow occurs frequently in industrial processes, especially in the petroleum and chemical industry. The fluid flow over the porous surface has lots of applications in filtration and purification processes, metal processing, heat exchangers, catalytic reactors,

insulation, etc. The physical concept of temperature variation between the plate and the surrounding fluid has many geothermal and engineering applications.

Blasius [36] initially investigated the development of velocity in the boundary layer when fluid flows past a planar surface. Pohlhausen [37] examined the Blasius heat transport mechanism. The numerical research on Blasius' findings regarding flow problems was further conducted by Kusukawa *et al*. [38]. Cheng and Minkowycz [39] presented the fluid flow in a porous media due to natural convection. Rabadi and Hamdan [40] demonstrated the natural convection fluid flow and heat transport over the inclined plate ingrained in a porous medium with the variation of permeability. Mukhopadhyay and Layek [41] studied numerically the convective heat transport mechanism of boundary layer fluid flow over a porous plate and analyzed the impact of radiation over temperature field.

Ishak [42] investigated the fluid motion and heat transport through a permeable plate considering convection heating at the boundary surface. Bhattacharyya *et al.* [43] examined numerically using the shooting method the fluid flow through boundary layer past a flat moving surface taking slip effects at the boundary. Bhattacharyya and Layek [44] also presented the solute diffusion due to the chemical reaction for boundary layer Newtonian fluid past a permeable plate. Abbas *et al.* [45] studied the heat transfer phenomenon taking slip condition at the boundary of viscous fluid past an infinite oscillating sheet. Khan *et al.* [46] demonstrated the heat transport and slip effects over a flat surface for carbon nanotubes. Ambreen *et al.* [47] discussed the heat transport and slip impact on hydromagnetic peristaltic non-Newtonian fluid flow. Sarojamma *et al.* [48] studied the stratified casson fluid motion and the heat transition taking radiation effect into account. Izadi *et al.* [49] presented the numerical solution of nanofluid containing microorganisms past a stretching sheet imposing slip condition and studied the heat transfer mechanism.

Inspired by the above researchers, this study intend to analyze the elastico-viscous boundary layer fluid flow and heat transport with partial slip effects over a porous flat plate. Walters Liquid (Model $B^{'}$) is considered for viscous and elastic characteristics. The self-similar reduced governing equations together with boundary conditions are evaluated employing MATLAB inbuilt solver ‘bvp4c’. The numerically generated results are accompanied by graphs analyzing the impact of multiple associated flow feature parameters.

2.2 Mathematical Formulation

The incompressible steady elastico-viscous fluid flow past a permeable flat plate with slip condition is investigated. The geometrical fluid flow model is displayed in Fig.2.1. The fluid flow is governed by the following equations.

$$u_x + v_y = 0 \tag{2.2.1}$$

$$uu_x + vu_y = \nu u_{yy} - \frac{k_0}{\rho}\left(uu_{xyy} + vu_{yyy} - u_y u_{xy} - v_y u_{yy}\right) - \frac{\nu}{k}(u - U_\infty) \tag{2.2.2}$$

$$uT_x + vT_y = \left(\frac{K}{\rho C_p}\right) T_y \tag{2.2.3}$$

where $\nu = \frac{\mu}{\rho}$.

The relevant boundary conditions taking slip effects are as follows:

$$u = G_1 u_y\,, v = v_w \text{ at } y = 0; \quad u \to U_\infty \text{ as } y \to \infty \tag{2.2.4}$$

$$T = T_W + H_1 T_y \text{ at } y = 0\ ;\ T \to T_\infty \text{ as } y \to \infty \tag{2.2.5}$$

where, $G_1 = G_0 (Re_x)^{\frac{1}{2}}$, $H_1 = H_0 (Re_x)^{\frac{1}{2}}$, $Re_x = \frac{U_\infty x}{\nu}$ $v_w = \frac{v_0}{(x)^{\frac{1}{2}}}$:

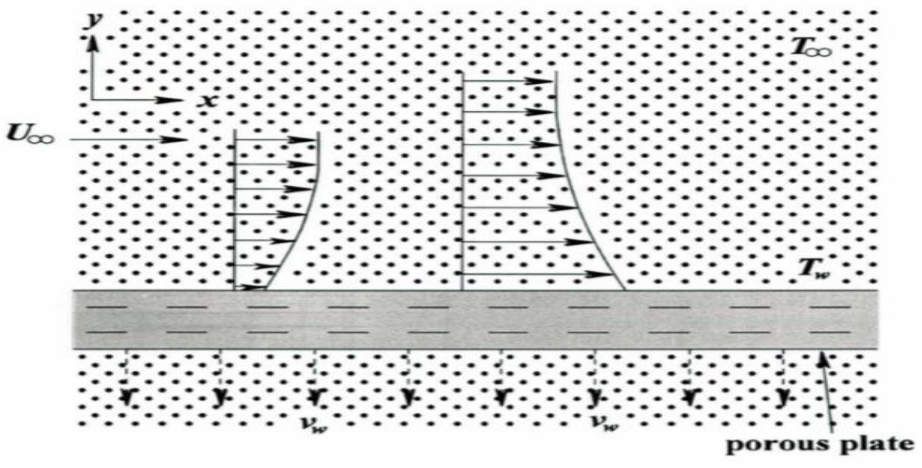

Fig. 2.1 Geometrical model of the flow problem

A careful inspection gives the following set of similarity transformations:

$$\Psi = \sqrt{U_\infty \nu x}\, f(\eta), T = T_\infty + (T_w - T_\infty)\theta(\eta), \text{ and } \eta = \frac{y}{x}\sqrt{Re_x}\,, \tag{2.2.6}$$

where Ψ denotes the stream function satisfying $u = \frac{\partial \Psi}{\partial y}$ and $v = -\frac{\partial \Psi}{\partial x}$.

Using similarity transformations, equations (2.2.6), (2.2.2) and (2.2.3) finally reduced to self-similar forms as follows:

$$f''' + \frac{1}{2} f f'' + k_1[2f'f''' + ff'^{\mathrm{v}} - (f'')^2] + k^*(1 - f') = 0 \tag{2.2.7}$$

$$\theta'' + \frac{1}{2} Prf\theta' = 0 \tag{2.2.8}$$

where dashes denote differentiation with respect to η and $k_1 = \frac{k_0 U_\infty}{2\mu x}$, $k^* = \frac{1}{Da_x Re_x}$, $Da_x = \frac{k}{x^2}$, $Pr = \frac{\mu C_p}{K}$.

The reduced form of boundary conditions (2.2.4) and (2.2.5) are:

$$f(\eta) = S,\ f'(\eta) = \delta f''(\eta)\ at\ \eta = 0\ ;\quad f'(\eta) = 1,\ f''(\eta) = 0\ as\ \eta \to \infty \tag{2.2.9}$$

$$\theta(\eta) = 1 + \beta\theta'(\eta)\ at\ \eta = 0\ ;\ \theta(\eta) = 0\ as\ \eta \to \infty \tag{2.2.10}$$

where, $S = \left(-\frac{2v_w}{U_\infty}\right)(Re_x)^{\frac{1}{2}} = -\frac{2,v_0}{(U_\infty \nu)^{\frac{1}{2}}}$, $S > 0$ (for $v_0 < 0$) represents suction and $S < 0$ (for $v_0 > 0$) represents blowing, $\delta = \frac{G_0 U_\infty}{\nu}$ and $\beta = \frac{H_0 U_\infty}{\nu}$.

2.3 Method of Solution

The self-similar governing equations (2.2.7) and (2.2.8) are transformed to differential equations of the first order as follows:

$$f = f_1, f' = f_2,\ f'' = f_3, f''' = f_4\ , \theta = f_5, \theta' = f_6 \tag{2.3.1}$$

From (2.3.1), we can write

$$f_1' = f_2,\ f_2' = f_3,\ f_3' = f_4,\ f_5' = f_6 \tag{2.3.2}$$

In view of equations (2.3.1) and (2.3.2), reduced governing equations (2.2.7) and (2.2.8) and boundary conditions (2.2.9) and (2.2.10) can be written as:

$$f_4' = \frac{1}{f_1}\left[(f_3)^2 - 2f_2 f_4 - \left(\frac{1}{k_1}\right)\left\{f_4 + \frac{1}{2} f_1 f_3 + k^*(1 - f_2)\right\}\right] \tag{2.3.3}$$

$$f_6' = -\frac{1}{2} Pr f_1 f_6 \tag{2.3.4}$$

$$f_1(0) = S, f_2(0) = \delta f_3(0) \; and \;\; f_2(\infty) = 1, f_3(\infty) = 0 \tag{2.3.5}$$

$$f_5(0) = 1 + \beta f_6(0) \;\; and \;\; f_5(\infty) = 0 \tag{2.3.6}$$

The MATLAB inbuilt solver 'bvp4c' is employed to compute the above equations together with different involved flow feature parameters.

2.4 Results and Discussion

The expression for friction at the surface for the above flow problem is obtained from

$$\tau = f''(0) + k_1 f(0) f'''(0) \tag{2.4.1}$$

The expressions for velocity $\left(f'(\eta)\right)$, temperature $\left(\theta(\eta)\right)$, temperature gradient $\left(-\theta'(0)\right)$ and skin friction coefficient (τ) are obtained numerically using MATLAB built-in 'bvp4c' solver for involved dimensionless flow parameters viz., elastico-viscous parameter (k_1), permeability parameter (k^*), velocity slip parameter (δ), suction/blowing parameter (S), thermal slip parameter (β) and Prandtl parameter (Pr). The computed results are graphically presented to observe the effects of involved flow parameters to explain the physical reasons.

To evaluate the precision of the numerical results obtained using 'bvp4c' and to validate the present work, the skin friction coefficient is evaluated without taking elastico-viscous and permeability parameters and is obtained as $f''(0) = 0.3321$ which is well accord with the standard results obtained by Howarth [50] as $f''(0) = 0.33206$ and Bhattacharyya and Layek [51] as $f''(0) = 0.332058$.

Fig. 2.2−2.5 illustrate the velocity distribution for variation of involved flow parameters. The velocity curves $f'(\eta)$ tends to 1 very rapidly as $\eta \rightarrow 3$ and thus considering 3 as infinity appears to justify the boundary conditions at infinity. Fig. 2.2 depicts the velocity curves for different incremental values of k_1 and it's clear that velocity $f'(\eta)$ enhances with the growth of $\mathrm{k}_1$and consequently diminishes the momentum boundary layer thickness. The thermal motion deforms the polymers of visco-elastic material and hence increase the fluid motion. Fig. 2.3 shows the effect of the permeability parameter k^* on the velocity curves. It is noticed that the velocity $f'(\eta)$ on the plate decelerates with rising values of k^*. With an increase in the permeability parameter, the Darcian body force decreases, resulting in a decrease in fluid motion. As the fluid is elastico-viscous so considerable high drag is accomplished and thus the velocity retarded. Fig. 2.4 displays the

velocity curves for suction parameters S and it is noticed that the flow rate decelerates with increasing values of S. As the particles of the fluid absorbed through the permeable plate, the fluid motion reduces and causes a reduction in the thickness of velocity boundary layer. The velocity profile $f'(\eta)$ for variation of slip factor δ is plotted in Fig. 2.5. The rate of fluid transport enhances as the slip factor δ rises due to frictional resistance between the fluid and the boundary surface. The positive values of velocity close to the plate is noticed due to slip and thus the thickness reduces for momentum boundary layer.

The temperature curves are graphically presented in Fig. 2.6 - 2.9 for various values of involved flow feature parameters. Fig. 2.6 shows that the fluid temperature reduces with the growth of k_1. As fluid becomes more viscous it hinders the transition of thermal energy to the fluid easily and thus temperature curves decrease. It signifies that the thermal boundary layer thickness diminishes with the growth of k_1. Fig. 2.7 demonstrates that the fluid temperature accelerates with the rise of permeability factor and thus we can conclude that the thickness of the thermal boundary enhances with the rising permeability. Growing permeability reduces the momentum boundary layer thickness and helps to enhance the fluid temperature. Fig. 2.8 depicts the temperature profile for various values of S. It is noticed that fluid temperature diminishes with growing values of suction. The thickness of thermal boundary layer decreases and thus heat transport increases. The growing values of suction bring fluid near to the plate and diminish the fluid temperature. Fig. 2.9 indicates that the fluid temperature diminishes as slip factor δ enhances and thus less amount of heat is deported from the porous plate to the fluid. A high rate of fluid motion is observed near the plate due to the slip factor which enhances the heat transfer.

The temperature gradient curves $\left(-\theta'(0)\right)$ against the velocity and thermal slip factors δ and β for variation of involved flow parameters are plotted in Fig. 2.10−2.13. It is noticed from Fig. 2.10 that as slip and elastico-viscous parameters enhance, the plate temperature rises. But, Fig. 2.11 shows that the heat transport rate enhances from the plate with growing elastico-viscous parameter but diminishes with increasing thermal slip parameter. Fig. 2.12 indicates that the heat transsition rate reduces with increasing permeability factor but enhances with the growth of slip flow parameter whereas, from Fig. 2.13, it is evident that the heat transition rate reduces with the growth of permeability and thermal slip parameters.

The determination of skin friction is very much important in engineering to estimate the total frictional drag exerted on the object and to evaluate the heat transition rate on its

surface. The friction (τ) on the surface of the plate is depicted in Fig. 2.14−2.15 against δ for several values of elastico-viscous and permeability parameters for fixed values of involved flow parameters. From Fig. 2.14, it is apparent that viscous drag on the surface enhances with the rising values of the elastico-viscous parameter and gradually diminishes with the growing slip parameters. The result is justified as increasing viscosity together with elasticity impede the forward movement of the fluid at the plate due to strong frictional drag. From Fig. 2.15, it is noticed that the friction at the surface reduces rapidly with the growth of permeability and thus more fluid passes through the plate and approaches to zero as slip parameters are enhanced.

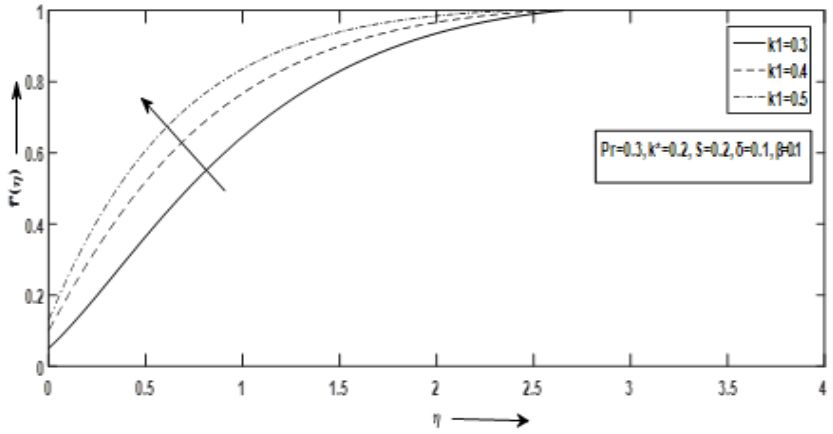

Fig. 2.2 Effects of k_1 on velocity curve $f'(\eta)$ against η

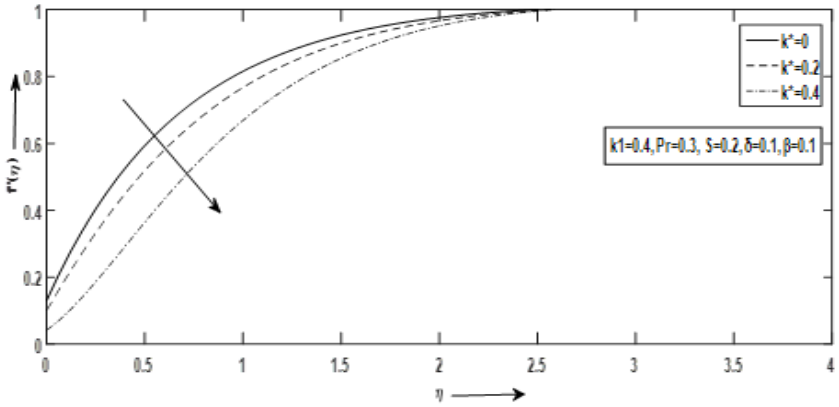

Fig. 2.3 Effects of k* on velocity $f'(\eta)$against η

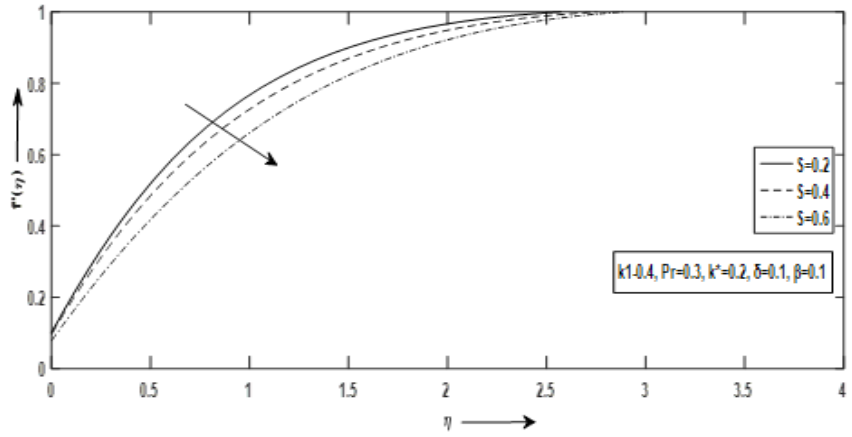

Fig. 2.4 Effects of S on velocity curve $f'(\eta)$ against η

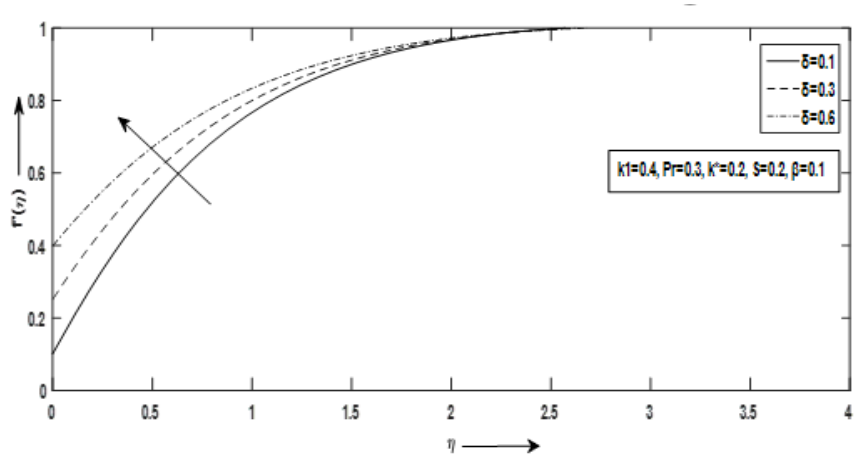

Fig. 2.5 Effects of δ on velocity curve $f'(\eta)$ against η

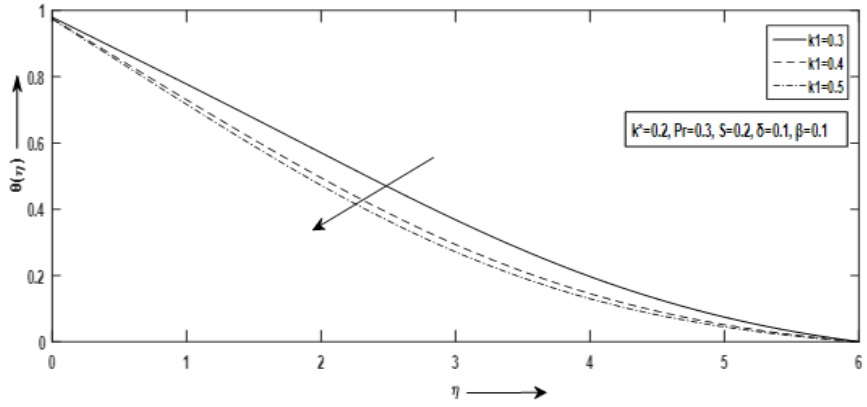

Fig. 2.6 Effects of k_1 on temperature curve (η) against η

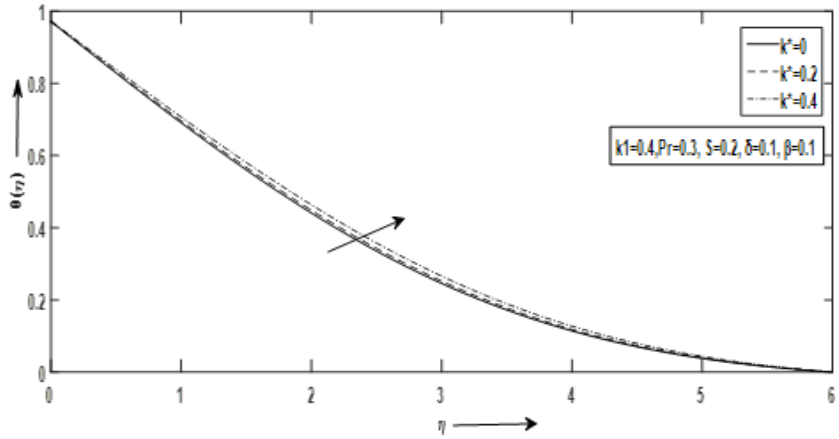

Fig. 2.7 Effects of k* on temperature curve (η) against η

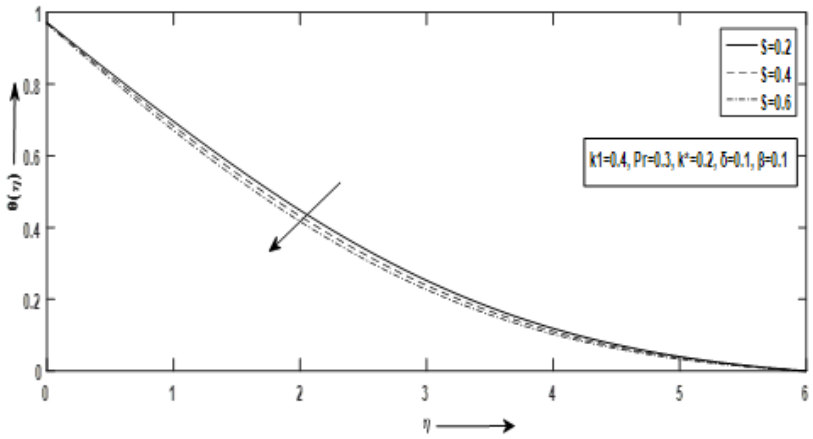

Fig. 2.8 Effects of S on temperature curve $\theta(\eta)$ against η

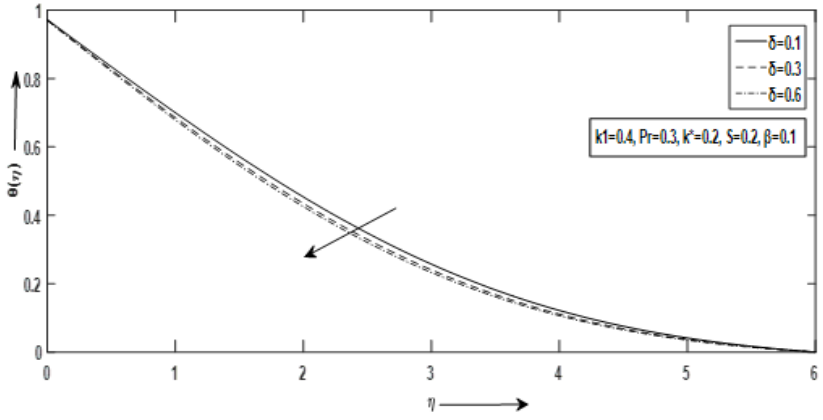

Fig. 2.9 Effects of δ on temperature curve $\theta(\eta)$ against η

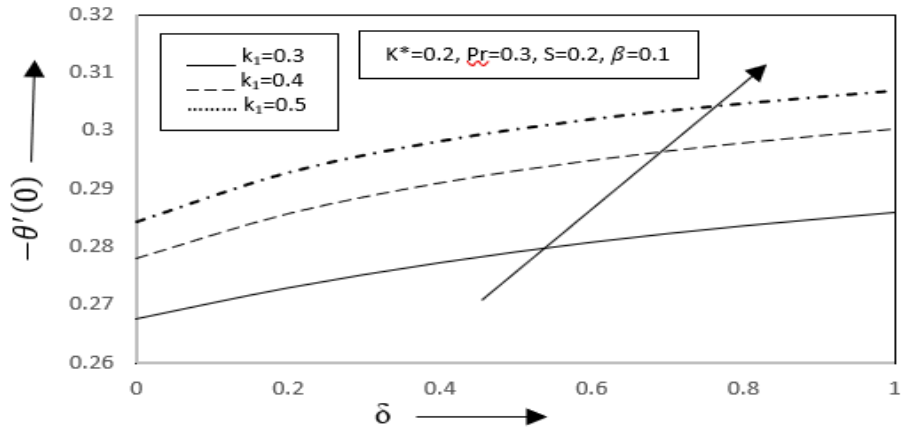

Fig. 2.10 Effects of $k_1$on temperature gradient curve$-\theta'(0)$ against δ

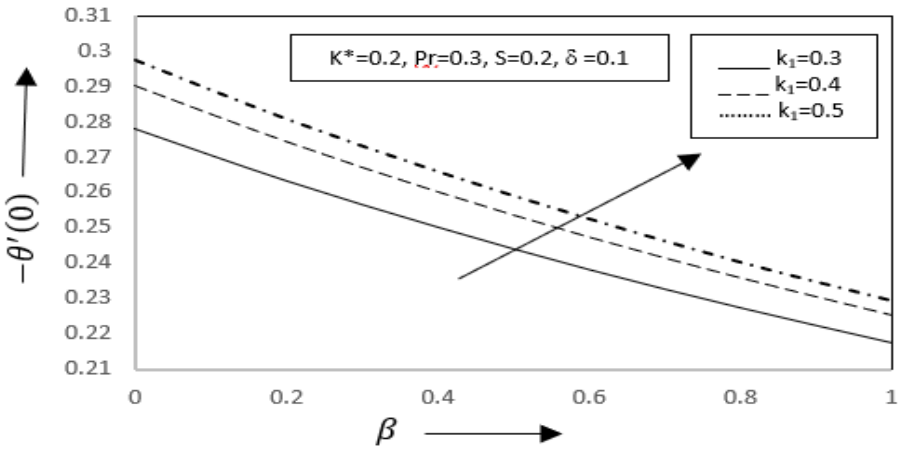

Fig. 2.11 Effects of k_1 on temperature gradient curve $-\theta'(0)$ against β

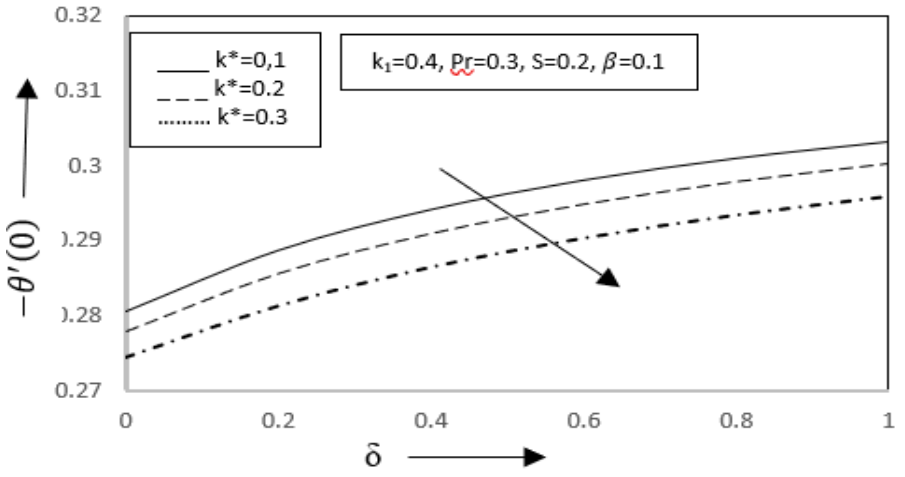

Fig. 2.12 Effects of k* on temperature gradient curve $-\theta'(0)$ against δ

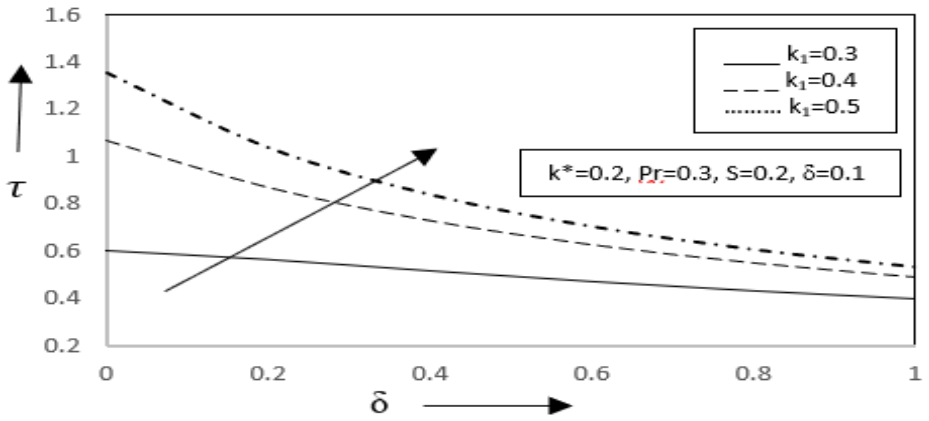

Fig. 2.14 Effects of k_1 on skin friction friction coefficient τ against δ

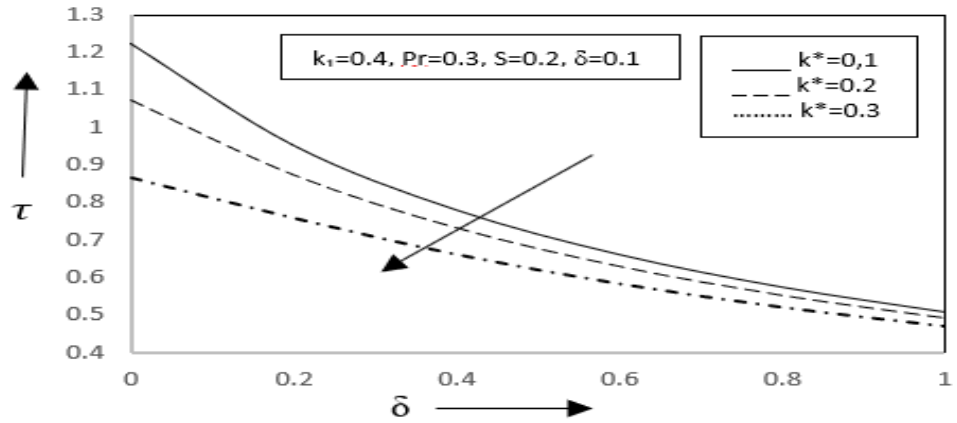

Fig. 2.15 Effects of k* on skin coefficient τ against δ

2.5 Conclusion

The study shows that elastico-viscosity plays an important role by reducing the drag on the flow to enhance the fluid velocity, heat transport rate and friction at the surface. The slip factor parameter role is also noticed to reduce the fluid temperature, heat transport rate and friction at the surface. The permeability parameter plays significant role to controlled the heat transition rate and the friction at the plate. The applied suction parameter brings fluid near to the plate and reduces the flow velocity and temperature of the fluid. A future investigation examining the problem's flow simulation and stability analysis would be extremely intriguing. A comparative study of the solution of the same problem using different numerical and analytical methods may also possible. It is expected that the physics of flow across a flat plate can be used from our study as the basis of many technological

and scientific applications. The findings of this study will be source of inspiration for future experimental work, which appears to be missing at the moment.